INTERNATIONAL JOURNAL OF PRECISION ENGINEERING AND MANUFACTURING Vol. 16, No. 10, pp. 2129-2137 SEPTEMBER 2015 / 2129
DOI: 10.1007/s12541-015-0275-y ISSN 2234-7593 (Print) / ISSN 2005-4602 (Online)

Modelling of the Hot Flow Behaviors for Ti-13Nb-13Zr Alloy by BP-ANN Model and Its Application

Guo-zheng Quan[1,#], Shi-ao Pu[1], Zong-yang Zhan[1], Zhen-yu Zou[1], Ying-ying Liu[1], and Yu-feng Xia[1]

1 State Key Laboratory of Mechanical Transmission, School of Material Science and Engineering, Chongqing University, Chongqing, 400044, China
Corresponding Author / E-mail: quanguozheng@cqu.edu.cn, TEL: +86-159-2290-0904, FAX: +86-023-6511-1493

KEYWORDS: Titanium alloy, Flow stress, Model, Backpropagational artificial neural network, Finite element

The plastic deformation mechanisms and the constitutive model of flow behaviors at different deformation conditions in biomedical titanium alloy are an essential step to optimize the design of any forging process for implant productions. A series of isothermal compressions tests on Ti-13Nb-13Zr alloy in a wide range of true strain, temperature and strain rate were conducted on a thermo-mechanical simulator. The hot flow behaviors with different softening mechanisms, including dynamic recrystallization and dynamic recovery, were characterized based on true strain-stress curves. A back-propagational artificial neural network (BP-ANN) method was conducted to evaluate and predict this non-linear problem by self-training to be adaptable to the material characteristics. The flow stress of this material a wide deformation condition range can be predicted accurately by the BP-ANN model obtained in this study. The prediction ability of this BP-ANN Model was evaluated by three accuracy indexes, Absolute error, Relative error and Average absolute relative error. Sequently, the developed BP-ANN model was programed and implanted into the finite element (FE) analysis platform, Msc.Marc software. The results have sufficiently articulated that the well-trained ANN model has excellent capability to deal with the complex flow behaviors and has great application potentiality in hot deformation processes.

Manuscript received: March 10, 2015 / Revised: June 8, 2015 / Accepted: July 4, 2015

1. Introduction

Titanium alloys are now extensively considered by medical professionals to be the metal of choice for the biomedical implants from head to toe such as prosthetics, internal fixation, inner body devices, instrumentation, etc.[1,2] This is due to their excellent properties such as low modulus, superior biocompatibility and enhanced corrosion resistance compared to more conventional stainless steels and cobalt chromium alloys.[2] The first generation of biomedical titanium alloy were $\alpha+\beta$ titanium alloys such as Ti-6Al-4V, Ti-6Al-7Nb and Ti-5Al-2.5Fe, which have been widely used as hard tissue replacements in artificial bones, joints and dental implants.[3,4] As for a new metal biomaterial employed to replace the bone, it is expected that the material has similar mechanical properties to bone. The $\alpha+\beta$ titanium alloys have some disadvantages: its elastic modulus, although low, is 4 to 6 times higher than cortical bone, and has low wear resistance that could not be suitable in articulations surfaces. This difference of rigidity produces the stress-shielding phenomenon due to the mismatch between the stiffness of the bone and that of the metal implant stem.[5-7] In recent years, the second generation of titanium alloy biomaterials concerning metastable β-Ti alloys with lower modulus avoiding the stress-shielding phenomenon have been developed for orthopedic applications.[7-9] The human bone has a Young modulus of 7~25 GPa, while these new titanium alloys have an elastic modulus of 55~85 GPa. Although it is still stiffer than the cortical bone, it is more proximal to the bone modulus and minimize the stress shielding phenomena greatly.[7,10]

In this work, Ti-13Nb-13Zr has been used in orthopedic applications due to its low Young's modulus (40~80 GPa), non-toxic composition, high tensile strength of approximately 1300 MPa, and a superior corrosion resistance when compared to Ti-6Al-4V alloy.[11] For Ti-13 Nb-13Zr alloy, it is important to enhance the mechanical properties of titanium alloys to increase the lifetime of implant via plastic deformation techniques. The deep understanding of the hot flow behaviors of this alloy contributes to the design in various forming processes. How to model the hot flow pattern of the alloy is a significant issue ensuring the accuracy of simulation analysis as well as the kinetics of metallurgical transformation.[12] Developing a constitutive model for Ti-13Nb-13Zr alloy not only can characterize the stress-strain data collected from isothermal hot compression tests, but also can predict the data which are out of the experiment conditions. Furtherly, it is significant that this

model can be embedded in the finite element (FE) analysis software to get the accurate simulation for this alloy.

In this regard, application of accurate models capable of incorporating the most important processing parameters and solving highly non-linear complex problems is highly desirable. In recent years, it is commonly accepted that the artificial neural network (ANN), a computational tool based on the properties of biological neural systems, is a powerful tool extensively used in the development of nonlinear constitutive relationships.[13] ANN is a kind of data-driven black-box model, thus doesn't need explicit physical knowledge of deformation mechanisms but a collection of representative examples from the desired mapping functions for training.[14] Most ANNs contain some form of 'learning rule' which modifies the weights of the connections according to the input patterns that it is presented with. There are many different kinds of learning rules used by neural networks, while the delta rule is often utilized by the most common class of ANNs called backpropagational artificial neural network' (BP-ANN). With BP, 'learning' is a supervised process that occurs with each cycle through the forward activation flow of outputs, and the backwards error propagation of weight adjustments.[15] It is a common method of training artificial neural networks used in conjunction with an optimization method such as gradient descent. Recently, much attention has been paid to the constitutive description of the hot deformation behaviors of several alloys by BP-ANN model.[15,16-20] L. Cheng et al.,[16] X. Ma et al.,[17] A. Kumar et al.,[18] G. Srinivasu et al.,[19] Y. Sun et al.,[20] G. Z. Quan et al.[14] conducted BP-ANN models to predict the flow behaviors of Ti-45Al-8Nb, Ti17, Ti-6Al-4V, Ti-10V-4.5Fe-3Al, Ti-47Al-2Nb-2Cr, Ti-6Al-2Zr-1Mo-1V, etc. titanium alloys. These reports about BP-ANN reveal that BP-ANN is an effective tool to predict the complex non-linear hot flow behaviors by self-training to be adaptable to the material characteristics.

In this study, a series of compression tests on Ti-13Nb-13Zr biomedical titanium alloy were conducted in a wide true strain range of 0~0.92, a wide temperature range of 923 K~1173 K crossing the β-transus, and a wide strain rate range of 0.01~10 s^{-1}. The characteristics of the hot flow hehaviors with different softening mechanisms were described in details. Then, an appropriate BP-ANN model to characterize and predict the complex hot flow behaviors of Ti-13Nb-13Zr alloy was established, in which temperature, strain and strain rate were used as inputs of the artificial neural network, while flow stress was defined as the output. In further, the predictive power of this BP-ANN Model was evaluated by three accuracy indexes, Absolute error, Relative error and Average absolute relative error (AARE). It is more valuable that the developed BP-ANN model was programed by FORTRAN language, and then implanted into the FE analysis platform, Msc.Marc software, through the interface of 'URPFLO' subroutine. The comparison between the experimental load-displacement curve and simulated one was conducted, which illustrated that the developed BP-ANN model can be applied to simulate the hot forming processes of Ti-13Nb-13Zr alloy with high loading accuracy.

2. Flow Behavior Measurement and Results

2.1 Experimental procedures

The chemical composition (wt.%) of Ti-13Nb-13Zr alloy investigated in this paper is as follows: Nb-14.6, Zr-13.3, Fe-0.02, N-0.015, C-0.03, Ti-balance. The alloy was beta-solution treated at 1073 K (β transus at which $\alpha+\beta\rightarrow\beta$: ~1015 K) for 30 min and then quenched in water to obtain initial martensite microstructure. The homogenized ingot was scalped to 10 mm in diameter and 12 mm in height, and twenty-five such cylindrical specimens were prepared as shown Fig. 1. Hot compression tests were conducted on a computer-controlled, servo-hydraulic Gleeble 1500 machine which can be programmed to simulate both thermal and mechanical industrial process variables for a wide range of hot deformation conditions. The deformed specimens were heated to the deformation temperature at a heating rate of 30 K/s and held at that temperature for 180 s by thermo-coupled-feedback-controlled AC current. The compression tests corresponding to a height reduction ratio of 60% (true strain of 0.92) were conducted under isothermal conditions at six different temperatures of 923 K, 973 K, 1023 K, 1073 K, 1123 K and 1173 K, and four different strain rates of 0.01 s^{-1}, 0.1 s^{-1}, 1 s^{-1} and 10 s^{-1}. During the compression process, the load and displacement were measured, meanwhile the variations of true stress and true strain were monitored continuously by a personal computer equipped with an automatic data acquisition system. The true stress and true strain were derived from the measurement of nominal stress-strain relationship according to the following formula: $\sigma_T = \sigma_N(1-\varepsilon_N)$, $\varepsilon_T = \ln(1-\varepsilon_N)$, where σ_T is the true stress, σ_N the nominal stress, ε_T the true strain and ε_N the nominal strain.[14]

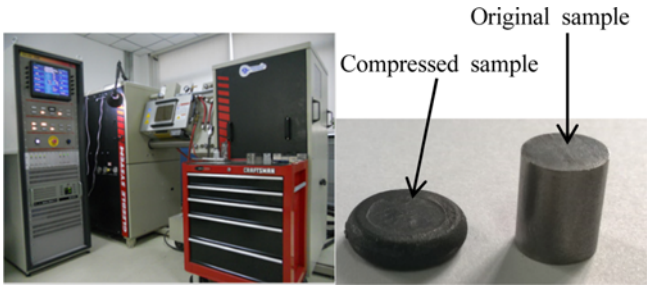

Fig. 1 the experimental setup and the specimens

2.2 Flow behavior characteristics

The true compressive stress-strain curves for Ti-13Nb-13Zr alloy at different temperatures and strain rates are illustrated in Fig. 2(a)~(d). It is clearly summarized that deformation temperature, strain rate and deformation degree (i.e., strain) have great influence on the flow stress of Ti-13Nb-13Zr alloy. By comparing these curves with one another, it is found that the peak stress of flow stress level monotonously decreases with an increase of deformation temperature at fixed strain rate and a decrease of strain rate at same temperature. This is mainly due to the fact that lower strain rate provides longer time for energy accumulation, as well as higher deformation temperature promotes the mobility at boundaries for the annihilation of dislocations or the nucleation and growth of dynamically recrystallized grains, and thus reduce flow stress level.

The exprimental temperature range of 923~1173 K crosses the β-transus, 1015 K, of Ti-13Nb-13Zr alloy. At β-transus, an allotropic phase transformation sustains changing from a hexagonal close-packed (hcp) crystal structure (α-phase) to a body-centered cubic (bcc) crystal

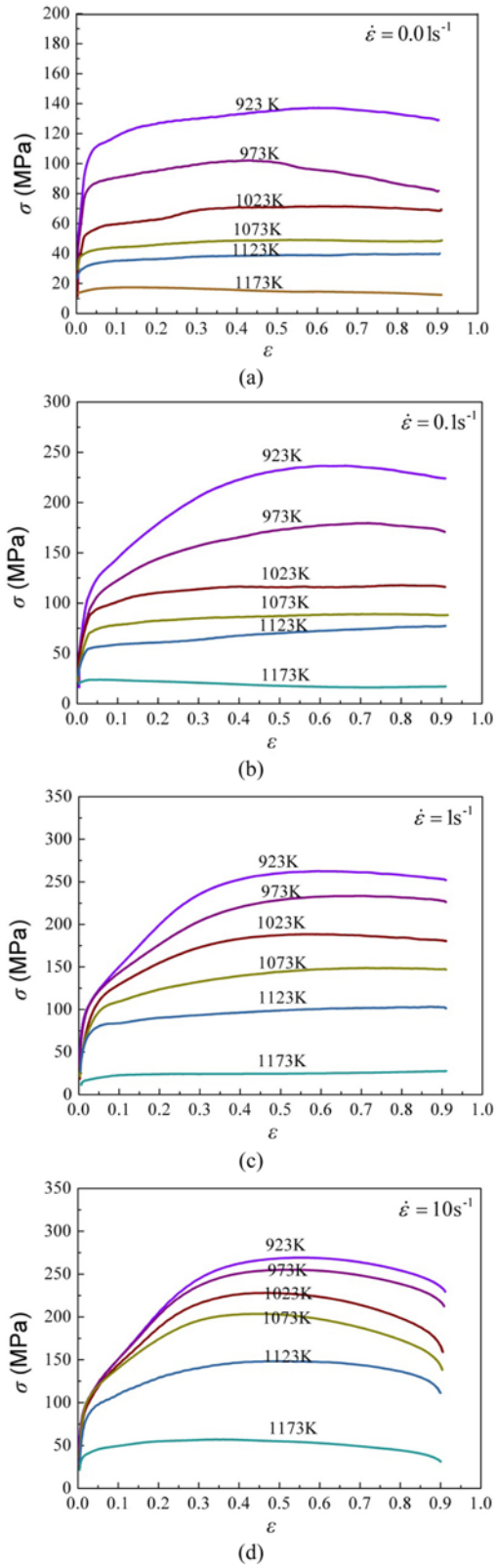

Fig. 2 The true stress-strain curves of Ti-13Nb-13Zr alloy under different temperatures with the strain rates of (a) 0.01 s^{-1}, (b) 0.1 s^{-1}, (c) 1 s^{-1}, (d) 10 s^{-1}

structure (β-phase). In common, when the temperature is lower than β transus, α-phase is the primary microstructure type coexisting with β-phase. When the temperature is above β-transus, phase transformation has been completed and only β-phase exists.[14] In α+β two-phase temperature range, flow stress increases with deformation degree extending until a peak stress value, following which decreases gradually to a steady value. Such flow behavior indicates obvious DRX softening mechanism. In β-phase temperature range, flow stress reaches rapidly a constant value with deformation degree extending. Such flow behavior indicates obvious DRV softening mechanism. According to the basis of DRV- or DRX-type flow behavior, from Fig. 2(a)~(d) it is identified that in the parameter domains of 0.01~10 s^{-1} & 1123~1173 K, 0.01~0.1 s^{-1} & 1023~1073 K, 1 s^{-1} & 1073 K, the corresponding stress-strain curves indicate DRV-type flow behavior of single β-phase, meanwhile in left parameter domains, the curves indicate DRX-type flow behavior of α+β two-phase. It is clear that in the parameter domains of 1~10 s^{-1} & 1023 K, 10 s^{-1} & 1073 K, although deformation temperatures are above β-transus, the corresponding stress-strain curves indicate DRX-type flow behavior of α+β two-phase. This can be attributed to decreased mobility of grain boundaries (growth kinetics) with increasing strain rate and decreasing temperature. Thus, under higher strain rates and lower temperatures, the deformed metal tends to DRX, on the contrary, tends to DRV. Such facts promote a very significant deduction that as for Ti-13Nb-13Zr alloy, temperature and strain rate are two main factors to determine the softening type of flow behaviors.

An allotropic phase transformation from α phase to β phase occurred at 1015 K, changing from a hexagonal close-packed (hcp) crystal structure (α phase) at lower temperatures to a body-centered cubic (bcc) crystal structure (β phase) at higher temperatures. hcp crystals slip is permitted with a-type slip directions on basal, prismatic and pyramidal planes and c + a-type slip directions on pyramidal planes. The basal and prismatic planes with a-type <11$\bar{2}$0> burgers vector only comprise four independent systems, and therefore there must be some additional slip or twinning systems to account for the fifth independent system. For higher temperature, bcc metals have a single well-defined close packed <111> direction, but several planes of equally high density of packing, i.e. {112}, {110}, {123}. The choice of slip plane in these metals is often influenced by temperature and a preference is shown for {112} below Tm/4, {110} from Tm/4 to Tm/2 and {123} at high temperatures. The non-basal slips increase with increasing temperature due to the fact that they are strongly thermally activated. Therefore, at relatively lower temperature, hot deformation behavior of the deformed material presents distinct DRX softening where α phase predominates, while DRV softening is obvious where β phase predominates.

3. Constitutive Modeling by BP-ANN

3.1 Basis of BP-ANN

To model the non-linear relationships between stress and three deforming parameters including temperature (T), strain (ε) and strain rate ($\dot{\varepsilon}$) by ANN, in common such three deforming parameters are considered as input variables, and stress (σ) as an output variable. A general schematic of ANN model for investigating the flow behaviors of an alloy is shown in Fig. 3.[18] Typically, the structure of an ANN model is hierarchical with neurons grouped in different layers involving an input layer, one or more hidden layers and an output layer. The input layer is used to receive data from outside, while the output layer is used

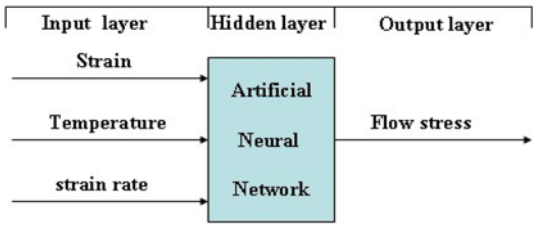

Fig. 3 Schematic of ANN structure in flow stress prediction

to generate output signals. The numbers of units at input and output layers are determined by the task at hand. Input layer units correspond to the number of independent variables, while output layer units correspond to the dependent variables or the predicated values. The hidden layers, which contain a systematically network of processing elements, are responsible for finding the non-linear features in complex problems. The numbers of hidden layers and the units in each layer may vary so as to minimize inefficiency in learning process and to maintain convergence rate, and must be testified. A network with fewer than the required number of hidden units will be unable to learn the input-output mapping, whereas too many hiden units will generalize poorly of any unseen data.[12-22] In this work, two hidden layers are favorable enough to describe the relationships between the hot flow behaviors and main process parameters.

In common a BP-ANN network is actually composed of two neural network algorithms, i.e., feed forward and back propagation, as shown in Fig. 4.[15] The BP method calculates the gradient of a loss function with respects to all the weights in the network. It requires a known, desired output for each input value in order to calculate the loss function gradient. The gradient is fed to the optimization method which in turn uses it to adjust the weights, in an attempt to minimize the loss function. The process of adapting the weights to an optimum set of values is called training the neural network. This involves series of optimizing loops backwards from the output layer all the way back to the input layer. Through a number of iteration, the loss function gradient will reach to minimum. Then, training could be ended.[12-22]

3.2 Development of BP-ANN Model

The total twenty-four true stress-strain curves of Ti-13Nb-13Zr alloy under six different temperatures and four different strain rates were divided into training set and testing set. The testing set included the curves under 923 K & 0.01 s^{-1}, 1123 K & 0.01 s^{-1}, 1073 K & 0.1 s^{-1}, 973 K & 1 s^{-1}, and 1023 K & 10 s^{-1}. The left curves belonged to the training set. And then, each continuous stress-strain curve was discretely handled by strain parameter from 0.03 to 0.9 at an interval of 0.03. Thus, total 720 data points on the twenty-four true stress-strain curves were collected. Furtherly, 80% data points (570) were gathered into the training dataset, and the left were gathered into the testing dataset.

However, the data carrying different units indicates the arbitrary effect of similarity between the objects, and a specific factor maybe dominates the learning for the BP-ANN model. This fact significantly decreases the convergence speed and accuracy within the network. Therefore, before network training, an essential step, the dimensionless normalization of all the measured data in the stress-strain measuring system including temperature, stress, strain and strain rate, must be

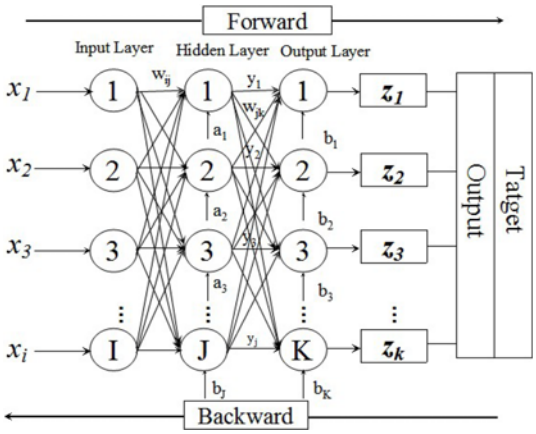

Fig. 4 Schematic illustration of BP-ANN network architecture

performed. Dimensionless normalization is the partial or full removal of the physical quantities' units from an equation by suitable substitutions within proper ranges. From the stress-strain curves as shown in Fig. 2, it can be seen that the measured strain data vary from 0.03 to 0.9, temperature data varying from 923 K to 1173 K, strain rate data varying from 0.01 s^{-1} to 10 s^{-1}, and the output flow stress data varying from 12.53 MPa to 269.54 MPa. In this work, the input parameters (temperature, strain and strain rate) were normalized as bare numbers within the range from 0 to 0.25 by the relation given by Eq. (1), and the output parameter (flow stress) was normalized as a bare number within the range from 0 to 1 by the relation given by Eq. (2).[23,24]

$$y_n = 0.25 \times \frac{y - 0.95y_{min}}{1.05y_{max} - 0.95y_{min}} \tag{1}$$

$$y_n = \frac{y - 0.95y_{min}}{1.05y_{max} - 0.95y_{min}} \tag{2}$$

where, y_n is the normalized value of y, y the experimental data, y_{max} the maximum value of y, y_{min} the minimum value of y.

As mentioned above, in the current model, two hidden layers are adopted to ensure high training accuracy. In the following, a very complex work of the structural parameter setting in BP-ANN model is essential. It involves an appropriate transfer function, an appropriate training function and an appropriate neuron number for each hidden layer. The neuron number for each hidden layer is often settled by a trail-and-error procedure according to the experience of designers. In addition, the determination of neuron number also has a direct relationship with the training sample number. With the increase of training sample number, the neuron number for each hidden layer should be increased. In order to approach the proposed accuracy, at beginning, the BP-ANN model was trained with only two neurons for each hidden layer, and then the neuron number was adjusted continually (three, four, etc.). The selected transfer function is 'Tansig' for each hidden layer, and 'Purelin' for output layer. In addition, the selected training function is 'trainbr'. In order to determine the neuron number for each hidden layer, an evaluator, sum square error (SSE) between experimental and predicted values is introduced into this work to evaluate the performance of the BP-ANN training work. SSE is expressed as Eq. (3).[25,26] Here, the proposed accuracy, i.e. the maximum SSE-value is set as 0.001.

$$SSE = \sum_{i=1}^{N}(E_i - P_i)^2 \quad (3)$$

where, E_i is the sample of experimental value; P_i is the sample of predicted value by the BP-ANN model; N is the number of true stress-strain samples.

As a series of BP-ANN models with different neuron numbers had been trained, the SSE-value corresponding to each actual training work was calculated. Thus, the difference between each calculated SSE-value and the preset SSE-value, here 0.001, was analyzed. The comparisions showed that the minimum difference was achieved when the neuron number in the first hidden layer meets 10, and it in the second hidden layer meets 12.

3.3 Prediction by BP-ANN Model

As the BP-ANN model had been evaluated, the complex flow behaviors with different softening rates of Ti-13Nb-13Zr alloy were predicted in a wide deforming parameter window. Fig. 5 shows the comparisons between the predicted flow stresses from BP-ANN model and the experimental ones. It can be seen that a satisfied agreement between the predicted and experimental data is achieved. The predicted flow stress tracks the work hardening and dynamic softening rate well, which suggests that the constructed BP-ANN model can describe the non-linear relationships among flow stress, strain rate, temperature and strain for Ti-13Nb-13Zr alloy.

In order to evaluate the predictive power of this BP-ANN Model, three accuracy indexes, Absolute error, Relative error and Average absolute relative error (AARE) were introduced into this work.[12-26] The former indicates the deviation between the predicted and experimental values expressed by Eq. (4). The middle indicates the ratio of the absolute error of the prediction to the accepted measurement expressed by Eq. (5). The last indicates the average value of the unsigned percentage error expressed by Eq. (6). The calculation results show that as for this BP-ANN model, the Absolute error varies from -19.45 to 16.34 (MPa), the Relative error varies from -12.99% to 9.33%, and AARE varies from 0 to 3.2%.

$$\text{Absolute error} = P_i - E_i \quad (4)$$

$$\text{Relative error}\ (\%) = \frac{P_i - E_i}{E_i} \times 100 \quad (5)$$

$$\text{AARE}(\%) = \frac{1}{N}\sum_{i=1}^{N}\left|\frac{E_i - P_i}{E_i}\right| \times 100 \quad (6)$$

where, E_i is the sample of experimental value; P_i is the sample of predicted value by the BP-ANN model; N is the number of true stress-strain samples.

In order to furtherly evaluate the strength of linear relationships between the experimental values and the predicted values of the training dataset with 570 data points, an evaluator, correlation coefficient (R) is introduced, and it is expressed by Eq. (7).[21-26] R is a numerical value between -1 and 1 that expresses the strength of the linear relationship between two variables. When R is closer to 1 it indicates a strong positive relationship. A value of 0 indicates that there is no relationship. Value close to -1 signal a strong negative relationship between the two

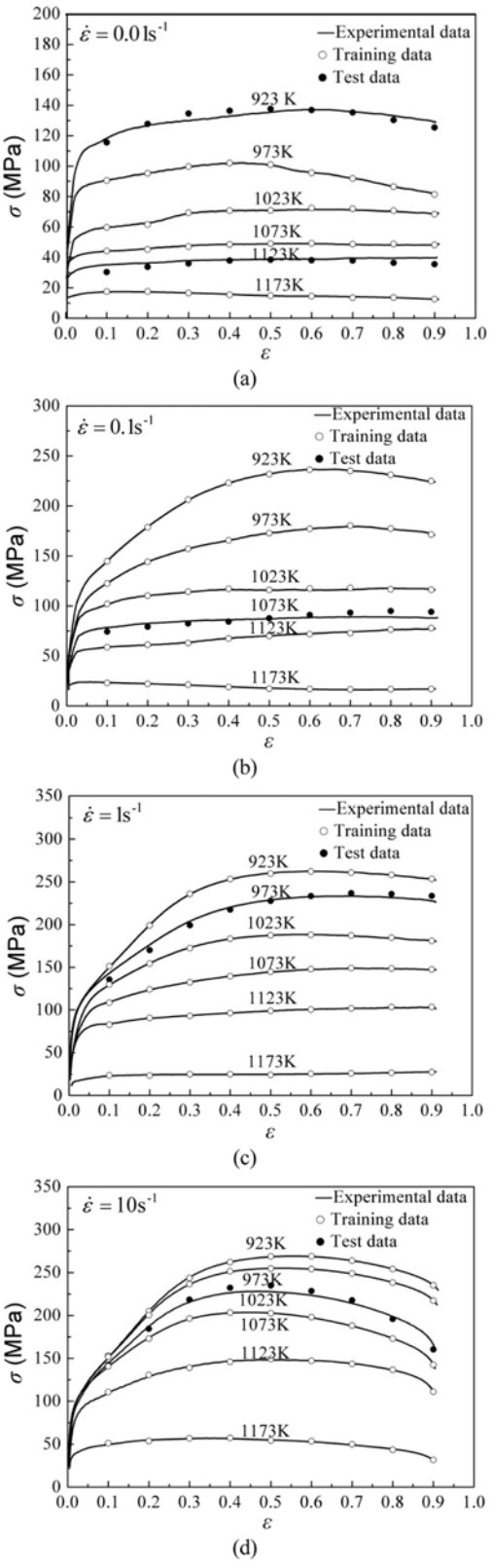

Fig. 5 Comparisons between the experimental and predicted flow stress by BP-ANN model of Ti-13Nb-13Zr alloy at different strains, strain rates and temperatures

variables. Fig. 6 shows the correlations between the experimental and the predicted flow stresses in both taining and testing processes, from which it can be seen that most of the data points lie fairly close to the

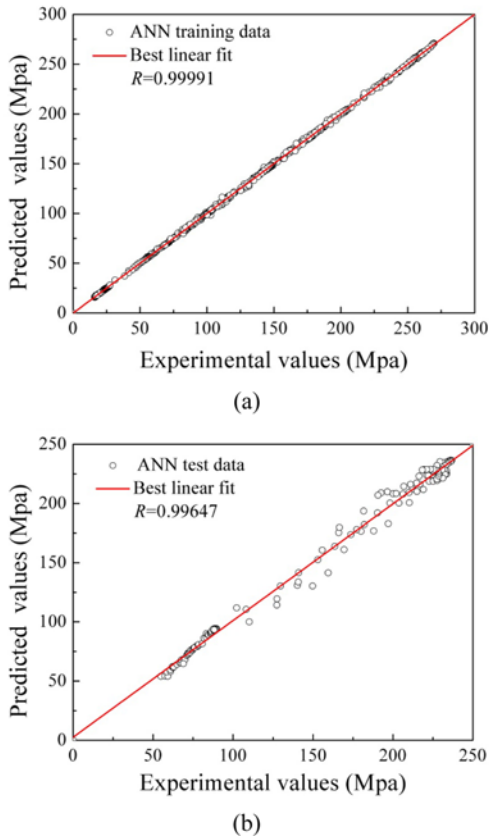

Fig. 6 Correlations between the predicted flow stress from BP-ANN and the experimental values: (a) in training process, (b) in testing process

best regression line. Apparently, the R-value for the training and testing dataset is 0.99991 and 0.99647 respectively. So to speak, in both taining and testing processes, the predicted stress data are highly correlated with the experimental data.

$$R=\frac{\Sigma_{i=1}^{N}(E_i-\overline{E})(P_i-\overline{P})}{\sqrt{\Sigma_{i=1}^{N}(E_i-\overline{E})^2\Sigma_{i=1}^{N}(P_i-\overline{P})^2}} \tag{7}$$

where E_i is the sample of experimental value; P_i is the sample of predicted value by the BP-ANN model; $\overline{E}$ is the mean value of experimental sample values; $\overline{P}$ is the mean value of predicted sample values; N is the number of true stress -strain samples.

4. Application Development of BP-ANN Model

4.1 Implanting BP-ANN Model into FE analysis

As we all know, the characterization of the flow behaviors of an alloy contributes significantly to its forming process design. Therefore, it can be said that the final purpose of modeling and prediction of these hot working state parameters is for the better practical use. In this work, an approach was developed to implant the desirable network into the FE analysis platform, Msc.Marc software. A neural network is essentially a 'black box' operation mapping the inputs of temperature, strain and strain rate to the output of flow stress using a particular set of non-linear basis functions. The essential step of reconstructing the above mapping relationships mathematically is to quantitate the so-called 'black box', i.e. the hidden layers and their interactions. Before starting this work, it is necessary to note the concept of simulation in BP-ANN model. The process utilizing the obtained network to predict wider mapping relationships is called as simulating the network. In whole, simulation is a single process of 'feed forward' during which each neuron processes the pattern and recalls patterns toward the direction of output layer, and finally outputs are returned. The implantation of the constructed BP-ANN model relies on the correct comprehension and compiling of the network architecture and simulation process. The arithmetic of 'feed forward' simulation process is expressed by Eqs. (8) ~(11),[27] and the developed corresponding program codes by FORTRAN language for implanting the constructed network into FE analysis platform are shown as Appendix 1. Thus, the constitutive model of flow behaviors for Ti-13Nb-13Zr alloy was further successfully implanted in the FE analysis software Msc.Marc though the interface of 'URPFLO' subroutine.

The input net_j of jth node of hidden layer:

$$net_j=\sum_{i=1}^{I}w_{ij}x_i+a_j \tag{8}$$

The output y_j of jth node of hidden layer:

$$y_j=\varphi(net_j)=\varphi\left(\sum_{i=1}^{I}w_{ij}x_i+a_j\right) \tag{9}$$

The input net_k of kth node of output layer:

$$net_k=\sum_{i=1}^{J}w_{jk}y_j+b_k=\sum_{i=1}^{q}w_{jk}\varphi\left(\sum_{i=1}^{I}w_{ij}x_i+a_j\right)+b_k \tag{10}$$

The output z_k of kth node of output layer:

$$z_k=\psi(net_k)=\psi\left(\sum_{i=1}^{J}w_{jk}y_j+b_k\right)=\psi\left(\sum_{i=1}^{q}w_{jk}\varphi\left(\sum_{i=1}^{I}w_{ij}x_i+a_j\right)+b_k\right) \tag{11}$$

where, x_i is the ith component of input vector; I, J, q are the neurons number of the input, hidden and output layer, respectively; a_j is the bias of jth neurons for the hidden layer, while b_k is the bias of kth neurons for the output layer; w_{ij} is the weight delivering from the ith neuron of output layer to the jth neuron of hidden layer, while w_{jk} is the weight delivering from the jth neuron of hidden layer to the kth neuron of output layer; net_j, net_k is the received value of the jth neuron of hidden layer and the kth neuron of output layer, respectively; φ, ψ is the transfer function of hidden layer (s) and output layer, respectively; y_j, z_k is the output of hidden layer (s) and output layer, respectively.

4.2 FE simulation on the platform with implanting network

The hot compression process with a height reduction ratio of 60% at temperature of 1073 K and strain rate of 0.1 s^{-1} was simulated on the FE analysis platform, Msc.Marc, implanted by the ANN constitutive model for Ti-13Nb-13Zr alloy. It is a significant work to make a comparison between the simulated load-displacement curve and the experimental one. As for the ANN constitutive model in the FE model, the true stress-strain data in the strain range of 0~0.03 were deleted, which means that rigid-plastic type constitutive model was adopted and the elastic deformation was ignored. In order to approximate the actual conditions of the hot isothermal compression test, the thermal radiation

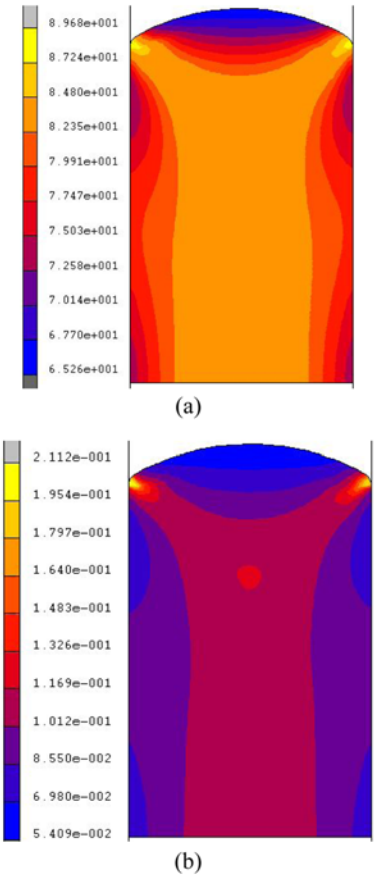

Fig. 7 The field distribution in the compressed material: (a) equivalent plastic strain, (b) equivalent plastic strain rate

and heat exchange among billet, anvils, and surrounding atmosphere were ignored. A shear friction coefficient of 0.1 was chosen to simulate the real graphite lubricant condition between the specimens and anvils. In order to maintain the constant strain rate of 0.1 s^{-1} in the compression, the movement of the moving anvil was set by a displacement control mode according to Eq. (12).[21]

$$L = L_0(1-\exp(-\dot{\varepsilon}t)) \tag{12}$$

where, L is the compression height amount of workpiece, which also equates with the displacement of the moving anvil; L_0 is the original height of workpiece, here 12 mm; $\dot{\varepsilon}$ is the expected constant strain rate; t is the compression time.

Figs. 7(a) and (b) shows the field distribution in the compressed material including the equivalent plastic strain and equivalent plastic strain rate. The inner center region of the compressed billet was chosen for the observation window. It can found that at the end of this compression the material in this region indicates an equivalent plastic strain rate of 0.1 s^{-1} or so, and an equivalent plastic strain of 0.92 or so. In whole, the simulated physical quantities shows a good agreement with the experimental conditions. The forming loads along with time or compression amount in the simulation process were collected, and then the load-displacement curve by simulation was plotted. As mentioned in previous, during the compression experiment, the variations of load and displacement were monitored continuously by an automatic data

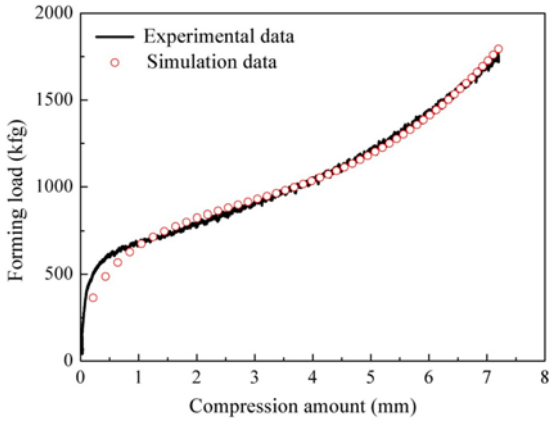

Fig. 8 Comparison between the experimental load-displacement curve and simulated one

acquisition system. Fig. 8 shows the comparison between the experimental load-displacement curve and simulated one, from which it can be seen that the experimental forming load approximates the simulated load all over the whole compressing process. It should be noted that the simulated load indicates relative larger tolerance when the compression amount, i.e. the displacement of anvil, is below 1 mm. This is due to the fact that in the BP-ANN model the initial training sample corresponds to the true strain of 0.03, and then the outward interpolation towards zero strain during the stress prediction corresponds to relative larger errors. However, most of metal forming process such as hot rolling, forging, extrusion relates to large deformations, thus the relative larger error in load at initial deforming stage makes very little effect to the follow-up deforming, and can be overlooked. All in all, the comparison between the experimental load-displacement curve and simulated one illustrates that the developed BP-ANN model can be applied to simulate the hot forming processes of Ti-13Nb-13Zr alloy with high loading accuracy.

5 Conclusions

An BP-ANN model has been suggested and conducted to evaluate and predict the deformation behaviors of as-cast Ti-13Nb-13Zr alloy using the experimental data from hot compression tests in a wide true strain range of 0~0.92, a wide temperature range of 923 K~1173 K crossing the β-transus, and a wide strain rate range of 0.01~10 s-1. The following conclusions were drawn:

(1) Under higher strain rates and lower temperatures, the deformed metal tends to DRX, on the contrary, tends to DRV. Temperature and strain rate are two main factors to determine the softening type of flow behaviors.

(2) Lower error level and higher R-value levels indicate that BP-ANN model has a good predictability under limited experimental conditions involving phase transformation.

(3) The developed BP-ANN model was programed into codes by FORTRAN language to be employed for simulation. The comparison between the experimental load-displacement curve and simulated one illustrates that the developed BP-ANN model can be applied to simulate

the hot forming processes of Ti-13Nb-13Zr alloy with high loading accuracy.

ACKNOWLEDGEMENT

This work was supported by Fundamental Research Funds for the Central Universities (CDJZR14135503).

REFERENCES

1. Chen, Q. and Thouas, G. A., "Metallic Implant Biomaterials," Materials Science and Engineering: R: Reports, Vol. 87, pp. 1-57, 2015.
2. Thieme, M., Wieters, K.-P., Bergner, F., Scharnweber, D., Worch, H., et al., "Titanium Powder Sintering for Preparation of a Porous Functionally Graded Material Destined for Orthopaedic Implants," Journal of Materials Science: Materials in Medicine, Vol. 12, No. 3, pp. 225-231, 2001.
3. Bordji, K., Jouzeau, J. Y., Mainard, D., Payan, E., Netter, P., et al., "Cytocompatibility of Ti-6Al-4V and Ti-5Al-2.5 Fe Alloys according to Three Surface Treatments, using Human Fibroblasts and Osteoblasts," Biomaterials, Vol. 17, No. 9, pp. 929-940, 1996.
4. Thair, L., Mudali, U. K., Rajagopalan, S., Asokamani, R., and Raj, B., "Surface Characterization of Passive Film Formed on Nitrogen Ion Implanted Ti-6Al-4V and Ti-6Al-7Nb Alloys using Sims," Corrosion science, Vol. 45, No. 9, pp. 1951-1967, 2003.
5. Niinomi, M., Nakai, M., and Hieda, J., "Development of New Metallic Alloys for Biomedical Applications," Acta Biomaterialia, Vol. 8, No. 11, pp. 3888-3903, 2012.
6. Gepreel, M. A.-H. and Niinomi, M., "Biocompatibility of Ti-Alloys for Long-Term Implantation," Journal of the Mechanical Behavior of Biomedical Materials, Vol. 20, pp. 407-415, 2013.
7. Navarro, M., Michiardi, A., Castano, O., and Planell, J., "Biomaterials in Orthopaedics," Journal of the Royal Society Interface, Vol. 5, No. 27, pp. 1137-1158, 2008.
8. Lee, Y.-S., Niinomi, M., Nakai, M., Narita, K., and Cho, K., "Predominant Factor Determining Wear Properties of β-type and (α +β)-Type Titanium Alloys in Metal-to-Metal Contact for Biomedical Applications," Journal of the Mechanical Behavior of Biomedical Materials, Vol. 41, pp. 208-220, 2015.
9. Akahori, T., Niinomi, M., Fukui, H., Ogawa, M., and Toda, H., "Improvement in Fatigue Characteristics of Newly Developed Beta Type Titanium Alloy for Biomedical Applications by Thermo-Mechanical Treatments," Materials Science and Engineering: C, Vol. 25, No. 3, pp. 248-254, 2005.
10. Henriques, V. A. R., Galvani, E. T., Petroni, S. L. G., Paula, M. S. M., and Lemos, T. G., "Production of Ti-13Nb-13Zr Alloy for Surgical Implants by Powder Metallurgy," Journal of Materials Science, Vol. 45, No. 21, pp. 5844-5850, 2010.
11. Müller, F. A., Bottino, M. C., Müller, L., Henriques, V. A., Lohbauer, U., et al., "In Vitro Apatite Formation on Chemically Treated (P/M) Ti-13Nb-13Zr," Dental Materials, Vol. 24, No. 1, pp. 50-56, 2008.
12. Quan, G.-Z., Li, G.-S., Wang, Y., Lv, W.-Q., Yu, C.-T., and Zhou, J., "A Characterization for the Flow Behavior of as-Extruded 7075 Aluminum Alloy by the Improved Arrhenius Model with Variable Parameters," Materials Research, Vol. 16, No. 1, pp. 19-27, 2013.
13. Basheer, I. A. and Hajmeer, M., "Artificial Neural Networks: Fundamentals, Computing, Design, and Application," Journal of Microbiological Methods, Vol. 43, No. 1, pp. 3-31, 2000.
14. Quan, G.-Z., Lv, W.-Q., Mao, Y.-P., Zhang, Y.-W., and Zhou, J., "Prediction of Flow Stress in a Wide Temperature Range Involving Phase Transformation for as-Cast Ti-6Al-2Zr-1Mo-1V Alloy by Artificial Neural Network," Materials & Design, Vol. 50, pp. 51-61, 2013.
15. Singh, S., Vashishtha, V., and Singla, T., "Artificial Neural Network," International Journal of Research, Vol. 1, No. 9, pp. 934-942, 2014.
16. Cheng, L., Chang, H., Tang, B., Kou, H. C., and Li, J. S., "Flow Stress Prediction of High-Nb Ti Al Alloys under High Temperature Deformation," Advanced Materials Research, pp. 723-728, 2012.
17. Ma, X., Zeng, W., Sun, Y., Wang, K., Lai, Y., and Zhou, Y., "Modeling Constitutive Relationship of Ti17 Titanium Alloy with Lamellar Starting Microstructure," Materials Science and Engineering: A, Vol. 538, pp. 182-189, 2012.
18. Kotkunde, N., Deole, A. D., Gupta, A. K., and Singh, S. K., "Comparative Study of Constitutive Modeling for Ti-6Al-4V Alloy at Low Strain Rates and Elevated Temperatures," Materials & Design, Vol. 55, pp. 999-1005, 2014.
19. Srinivasu, G., Rao, R. N., Nandy, T. K., and Bhattacharjee, A., "Artificial Neural Network Approach for Prediction of Titanium Alloy Stress-Strain Curve," Procedia Engineering, Vol. 38, pp. 3709-3714, 2012.
20. Sun, Y., Hu, L., and Ren, J., "Modeling the Constitutive Relationship of Powder Metallurgy Ti-47Al-2Nb-2Cr Alloy during Hot Deformation," Journal of Materials Engineering and Performance, Vol. 24, No. 3, pp. 1313-1321, 2015.
21. Quan, G.-Z., Liang, J.-T., Lv, W.-Q., Wu, D.-S., Liu, Y.-Y., Luo, G.-C., and Zhou, J., "A Characterization for the Constitutive Relationships of 42CrMo High Strength Steel by Artificial Neural Network and Its Application in Isothermal Deformation," Materials Research, Vol. 17, No. 5, pp. 1102-1114, 2014.
22. Quan, G.-Z., Yu, C.-T., Liu, Y.-Y., and Xia, Y.-F., "A Comparative Study on Improved Arrhenius-Type and Artificial Neural Network Models to Predict High-Temperature Flow Behaviors in 20 MnNiMo Alloy," The Scientific World Journal, Vol. 2014, Article ID: 108492, 2014.
23. Zhu, Y., Zeng, W., Sun, Y., Feng, F., and Zhou, Y., "Artificial Neural

Network Approach to Predict the Flow Stress in the Isothermal Compression of As-Cast TC21 Titanium Alloy," Computational Materials Science, Vol. 50, No. 5, pp. 1785-1790, 2011.

24. Gupta, A. K., Singh, S. K., Reddy, S., and Hariharan, G., "Prediction of Flow Stress in Dynamic Strain Aging Regime of Austenitic Stainless Steel 316 using Artificial Neural Network," Materials & Design, Vol. 35, pp. 589-595, 2012.
25. Chai, R.-X., Guo, C., and Yu, L., "Two Flowing Stress Models for Hot Deformation of XC45 Steel at High Temperature," Materials Science and Engineering: A, Vol. 534, pp. 101-110, 2012.
26. Mandal, S., Rakesh, V., Sivaprasad, P., Venugopal, S., and Kasiviswanathan, K., "Constitutive Equations to Predict High Temperature Flow Stress in a Ti-Modified Austenitic Stainless Steel," Materials Science and Engineering: A, Vol. 500, No. 1, pp. 114-121, 2009.
27. Vickram, A. S., Das, R., Srinivas, M. S., Rao, K. A., Jayaraman, G., and Sridharan, T., "Prediction of Zn Concentration in Human Seminal Plasma of Normospermia Samples by Artificial Neural Networks (ANN)," Journal of Assisted Reproduction and Genetics, Vol. 30, No. 4, pp. 453-459, 2013.

APPENDIX 1

The programe codes of the constructed network

Do i=1, M
$Net_1(1, i)=0$
DO j=1, 3
$Net_1(1, i)=IW_{21}(j, i)*X(1, j)+B_1(1, i)$
End do
$Y_1(1, i)=f_1(net_1(1, i))$
End do
Do i=1, N
$Net_2(1, i)=0$
DO j=1, M
$Net_2(1, i)=LW_{32}(j, i)*Y_1(1, j)+B_2(1, i)$
End do
$Y_2(1, i)=f_2(net_2(1, i))$
End do
$Net_3(1, 1)=0$
DO i=1,N
$Net_3(1, 1)=LW_{42}(i, 1)*Y_2(1, i)+B_3(1, 1)$
End do
$Output= f_3(net_3(1, 1))$

where, M and N are the corresponding neuron numbers of two hidden layers; i and j are the dynamic variables for loop computation; $X(1, 1)$, $X(1, 2)$, $X(1, 3)$ is the corresponding input component, namely temperature, strain and strain rate respectively; $Net_1(1, i)$, $Net_2(1, i)$ are the weighted input values of ith neurons of the two hidden layers; $Net_3(1, 1)$ is the weighted input value of the output neuron; $Y_1(1, i)$, $Y_2(1, i)$ are the output values of ith neurons of the two hidden layers; Output is the predicted value of the neural network, namely flow stress; B_1 is the bias vector for the first hidden layer, $net.b\{1\}$, a $N\times1$ cell array; B_2 is the bias vector for the second hidden layer, $net.b\{2\}$, a $M\times1$ cell array; B_3 is the bias vector for the output layer, $net.b\{3\}$ a 1×1 cell array; IW_{21} is the weight matrices of weights going to layers from network inputs, $net.IW\{2,1\}$, a $N\times3$ cell array; LW_{32} is the weight matrices of weights going to the second hidden layer from first hidden layer, $net.LW\{3,2\}$, a $M\times N$ cell array; LW_{42} is the weight matrices of weights going to the out layer from second hidden layer, $net.LW\{4,2\}$, a $N\times M$ cell array; f_1, f_2 and f_3 are the transfer function of two hidden layers and the output layer respectively.

For 'Tansig' transfer function (f_1 and f_2):

$$f(x)=\frac{2}{(1+\exp(-2^x))}-1 \quad (-1<x<1)$$

For 'Purelin' transfer function (f_3):

$$f(x)=x \quad (-1<x<1)$$